Hindawi
Journal of Sensors
Volume 2018, Article ID 1639387, 11 pages
https://doi.org/10.1155/2018/1639387

Research Article

Pulsed Eddy Current Nondestructive Testing for Defect Evaluation and Imaging of Automotive Lightweight Alloy Materials

Kai Zhang,[1] **Yunze He**,[2] **and Zhurong Dong**[1]

[1]*Automotive & Transportation Engineering, Shenzhen Polytechnic, Shenzhen 518055, China*
[2]*College of Electrical and Information Engineering, Hunan University, Changsha 410082, China*

Correspondence should be addressed to Kai Zhang; zhangkai@szpt.edu.cn

Received 15 September 2017; Revised 27 November 2017; Accepted 14 December 2017; Published 4 March 2018

Academic Editor: Stephane Evoy

Rapid and accurate damage detection of magnesium-aluminum alloy, which is an important material for automotive lightweight, is of great significance. Pulsed eddy current (PEC) is an effective electromagnetic nondestructive testing and evaluation (NDT&E) technique for metal materials. Metal loss evaluation and imaging are one of the most important steps in quality control and maintenance of key components of automobiles. A PEC method based on a rectangular excitation coil and an axial parallel pickup coil is proposed and investigated for the purpose of metal loss evaluation and imaging. Metal loss type of defects with different sections is designed and detected using line scanning technique and C-scan imaging in two scanning directions. Experimental results have illustrated that metal loss depth can be estimated effectively by the peak amplitude of PEC A-scan response. Then, the quantification information of metal loss depth is preliminarily obtained based on the linear fitting equation. Consequently, metal loss evaluation is realized by line scanning peak waves and C-scan pseudo 3D images. At last, the sensitivity comparison shows that the metal loss can be detected in both directions. The proposed method is an effective approach to evaluate the image surface-breaking metal loss in automotive lightweight alloy materials.

1. Introduction

Studies have shown that a lightweight vehicle is one of the most effective measures to reduce energy consumption and emissions. The development and application of lightweight materials is one of the main research directions of automotive lightweight. Their lightweight and very high specific stiffness provide great potential for vehicle weight reduction [1, 2]. Aluminum alloy and magnesium alloy materials have the characteristics of being lightweight, corrosion-resistant, and easy to process. It is a lightweight material widely used at present [3]. However, these new materials may sustain damage due to fatigue and mechanical collisions, such as entrained oxide film, which is invariably detrimental to the fatigue properties [4]. Casting defects such as blowhole, shrinkage cavity, and porosity easily occurred in aluminum alloy castings for automobiles. Figure 1 depicts the air holes ($0.5\sim5\,mm^3$) in the automobile air conditioner castings using X-ray and slice detection, respectively [5]. The effects of thixoforming defects on the stress-strain curves of the aluminum structural part and a shock tower part of a small electric vehicle were quantitatively investigated [6]. Therefore, it is of great value to study the nondestructive testing and evaluation (NDT&E) methods to evaluate and quantify the defects of these materials [7].

NDT is an excellent method for evaluating physical and mechanical properties [8], various defects, and other technical parameters of the interior or exterior of an object [9, 10]. Currently, many methods, such as X-ray testing, penetrant testing (PT), eddy current testing (ECT), magnetic particle testing (MT), ultrasonic testing (UT), acoustic emission testing (AET), and IR-thermography (IRT), are being used in the automotive industry. Among them, the research of solder joints and structural parts is in the majority [11–17]. Pulsed eddy current (PEC) is an effective NDT method for conductive materials [18–20]. Firstly, PEC testing does not require

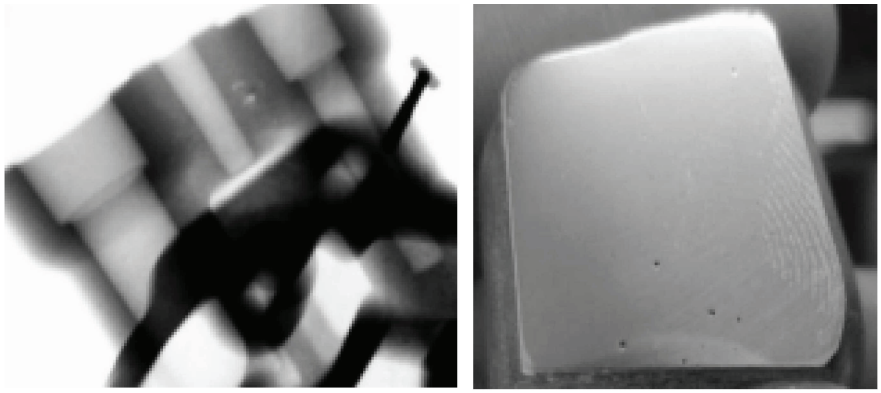

Figure 1: Blowhole of automobile aluminum alloy castings [5].

an acoustic couplant in contrast to ultrasonic inspection. Secondly, PEC is more economical and less hazardous than radiography. In addition, PEC testing boasts many advantages over conventional eddy current testing, including more extended detection depth and easier generation and control. PEC testing can be widely used to measure the thickness and stress [21] and to characterize crack, metal loss, and corrosion of metal materials and carbon fiber-reinforced plastic [22].

PEC testing technique also allows to measure the time-dependent response signal (A-scan response) and to analyze the response at different time points after pulse shut-off in order to gain information on the depth [23]. The rate of decay of the PEC A-scan transient is dependent on the total thickness of the structure and independent of lift-off and any gaps in the structure, just as the reference suggests [24]. We all know that lift-off is one of the biggest problems in ECT defect detection. PEC technique could be used to characterize material loss with gap and lift-off variations. This technique holds the potential of becoming the primary means of detecting corrosion in multilayered structures [25]. In 2002, Lepine et al. used the lift-off intersection (LOI) and gap point of time response to eliminate the lift-off effect and interlayer gap effect in the two-layer structures [26]. In recent years, some features from frequency response have been used to reduce these effects; He et al. used some FFT amplitude from PEC frequency response as a feature to classify the first-layer defects and second-layer defects in two-layer structures in 2010 [27, 28]. Principal component analysis (PCA) and independent component analysis (ICA) were also already used in PEC defect classification with lift-off effect [29, 30]. Pan et al. investigated the feature extraction from optimised frequency responses combining with PCA technique to overcome various air gaps and lift-off effect for defect classification in two-layer structures [31].

In PEC testing, the probe is usually comprised of the excitation unit and the detection unit. The excitation unit inducing eddy current in the material under test is usually a cylindrical coil. In contrast to cylindrical coils, a rectangular coil can induce a uniform eddy current in specimen [32] and has been particularly devised in both alternating current field measurement (ACFM) testing [33] and PEC testing [34]. The detection units detecting the magnetic field disturbed by the presence of a defect are various and multiform not only in its detecting principle, such as a magneto-resistive sensor [35], a giant magneto-resistive (GMR) sensor [36], a Hall-effect sensor [37], or a superconducting quantum interference device (SQUID) magnetometer [38], but also in its structure, such as a differential coil [39], multiple pickup sensors [40], or the three-dimensional coils [41]. The previous work has shown that the three-dimensional coils can offer more information about defect sizing and the pickup coil axial parallel to the excitation coil can quantify the defect's depth [41]. Therefore, the main objective of this paper is to investigate PEC testing based on the rectangular excitation coil and the axial parallel pickup coil for the purpose of metal loss evaluation and imaging.

At present, there are no public works on rectangular PEC testing method applied in the automotive industry. A novel method of PEC testing is discussed in this paper. The present study illustrates the possibility of metal loss shape evaluation using pulsed eddy current. Because of the hostile environment of automobiles, corrosion frequently occurs in metal components and will result in metal loss and wall thinning in many conditions. There is a big difference between these corrosions and mechanical damages. Therefore, metal loss evaluation and imaging are one of the most important steps. The rest of the paper is arranged as follows. Firstly, the PEC rectangular excitation coil and axial parallel pickup coil are introduced in Section 2. Next, experimental setup and specimen are shown in Section 3. Then, the line scanning-based metal loss evaluation is carried out in Section 4 and metal loss evaluation and sensitivity comparison based on C-scan imaging are investigated in Section 5. Finally, conclusions are outlined in Section 6.

2. Rectangular PEC Probe

As shown in Figure 2, the PEC probe in this work consists of a rectangular excitation coil and a cylindrical pickup coil. The pickup coil is also named B_x pickup coil, because it is normally parallel to the x-axis. The rectangular excitation coil can induce a uniform eddy current in the specimen, and the pickup coil axial parallel to the rectangular excitation coil

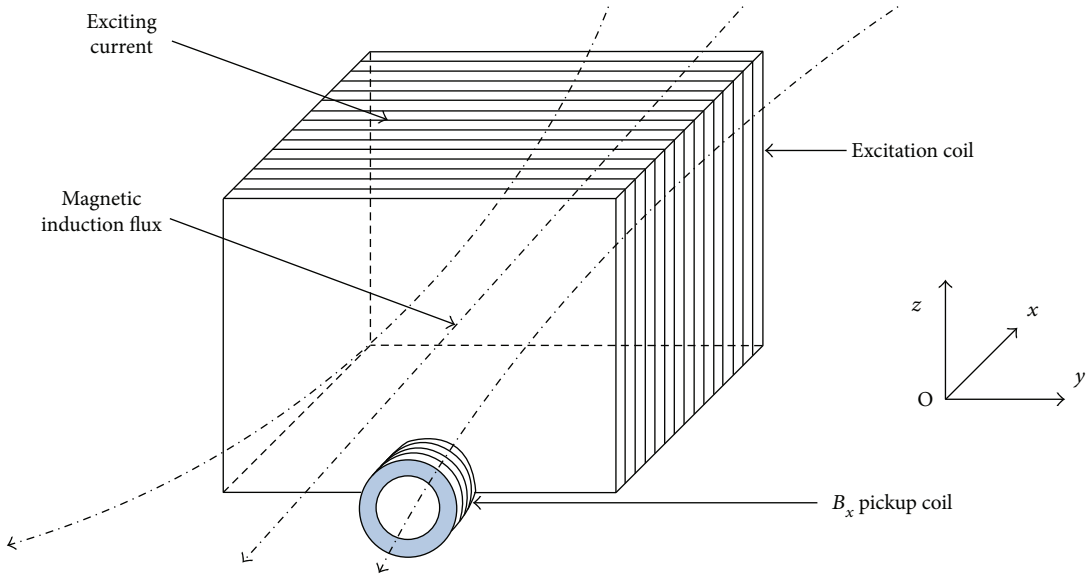

Figure 2: The rectangular excitation coil and axial parallel pickup coil.

Table 1: Parameters of the excitation coil and the pickup coil.

Parameters	Excitation coil	Pickup coil
Wire diameter (mm)	0.2	0.05
Number of turns	400	600
DC resistance (ohm)	40.2	39.21
Inductance (mH)	7.75	0.420

is located at the bottom center of the rectangular excitation coil to measure the rate of change of the magnetic field. The rectangular excitation coil is 50 mm in length, 45 mm in width, and 45 mm in height [42]. The lift-off of the probe is 0.5 mm, depending on the sensor core's dimensions. The other characteristics of the excitation coil and pickup coil are shown in Table 1. In previous work, the PEC sensor is scanned in two directions, one being the magnetic induction flux and the other being the excitation current [43]. In Figure 2, a Cartesian coordinate system is established. The direction of magnetic induction flux parallel with the x-axis is called X direction in the next work, whilst the direction of excitation current parallel with the y-axis is called Y direction. The experiments of metal loss evaluation in the next work are carried out in both directions.

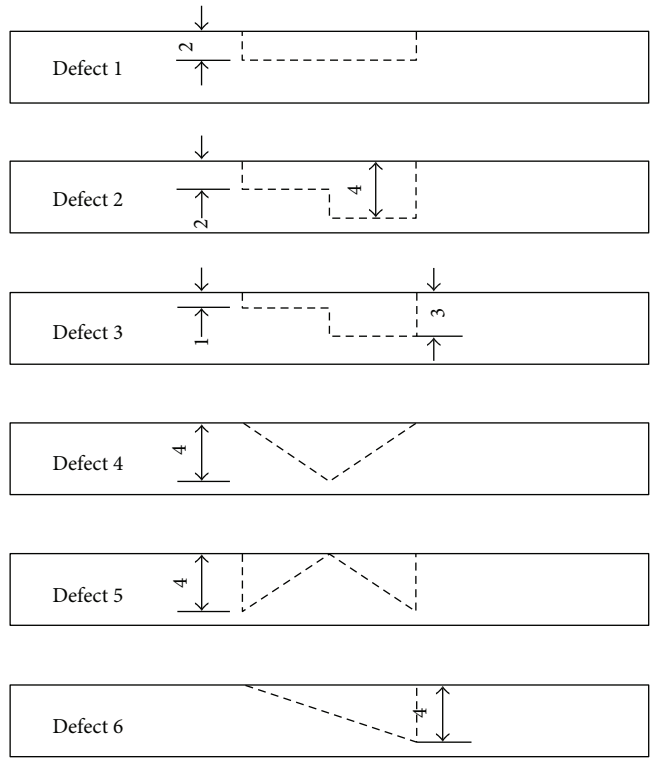

Figure 3: The sectional view of six defects.

3. Experimental Setup and Specimen

The PEC experimental setup in this work contains an excitation card, a signal conditioning card, and an analog to a digital converter card. The excitation pulse generated and enhanced by the excitation card is driven to a rectangular excitation coil. The response signal measured by the B_x pickup coil is amplified by the signal conditioning card and sampled by the data acquisition module to form the A-scan response in time domain. In this work, the excitation pulse is 7.5 V in amplitude, 100 Hz in frequency, and 5 ms in pulse duration. In experiments, only the peak amplitude is measured from A-scan response because this is the simplest method. In the future, other features including time-slices, peak time, and zero time in the time domain and zero-crossing frequency in the frequency domain will be used for defect detection [23]. In addition, it is widely known that the lift-off is one of the biggest problems for

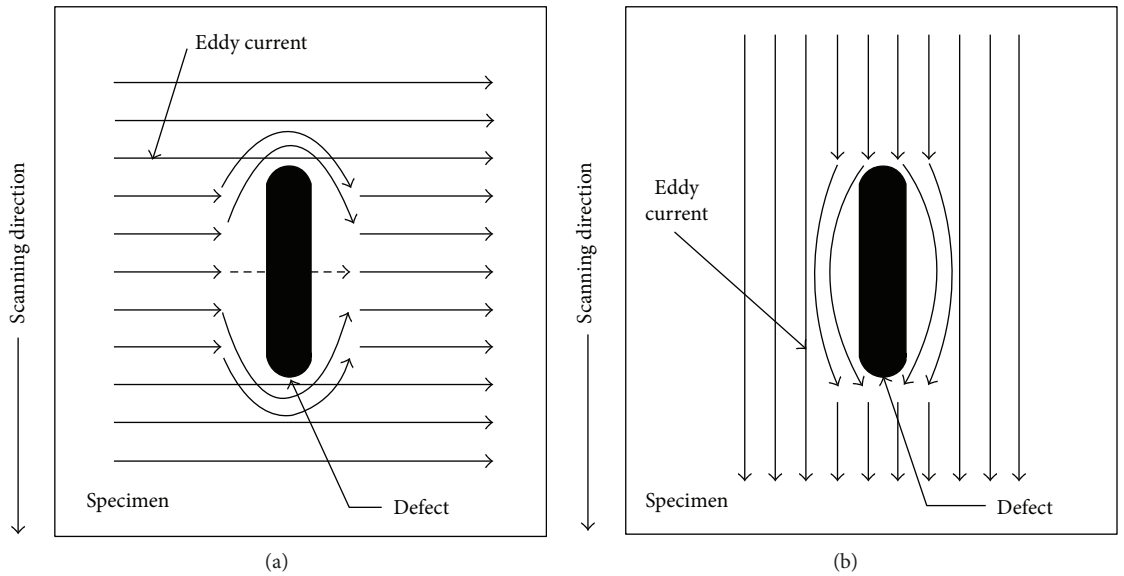

Figure 4: The eddy current disturbed by a defect in two directions. (a) Direction of magnetic induction flux. (b) Direction of excitation current.

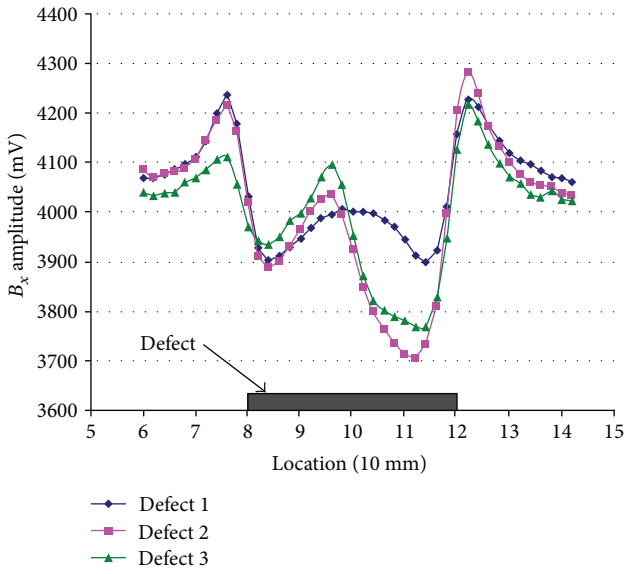

Figure 5: The line scanning peak waves of defects 1 to 3 in direction of magnetic induction flux.

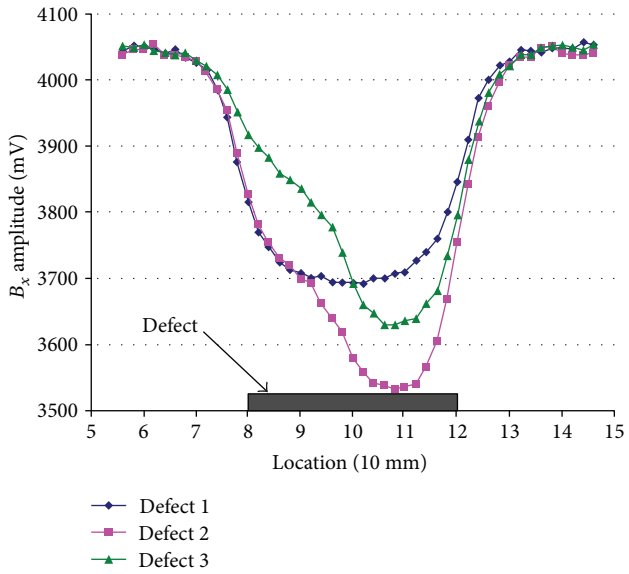

Figure 6: The line scanning peak waves of defects 1 to 3 in direction of excitation current.

pulsed eddy current sensors in applications [25]. In this work, the lift-off distance is always kept the smallest to eliminate the influence of lift-off effect as much as possible.

Six aluminum specimens with the length of 200 mm, width of 200 mm, and thickness of 5 mm are used to provide the surface-breaking metal loss type of defects in this paper. The material of the specimens is a 3A21 Al-Mn alloy (a widely used antirust aluminum alloy material, which is used in automobiles to make fuel tanks and conduits), whose conductivity is 50–55% IACS. On the surface of every specimen, an electron discharge machining (EDM) slot is manufactured to simulate metal loss with a different section. Each slot is 40 mm in length and 12 mm in width. Figure 3 shows the sectional view of all six defects (the unit is mm). Defect 1 is rectangular in section; defects 2 and 3 are stepped; defect 4 is wedge-shaped; defects 5 and 6 are triangular.

4. Line Scanning-Based Metal Loss Evaluation

4.1. Peak Waves in Both Directions. The PEC A-scan response can be obtained and then the peak amplitude can be extracted. When a PEC probe scans along a line, peak wave can be formed by the peak amplitude of all A-scan responses. In the direction of magnetic induction flux, when

Table 2: Peak amplitude corresponding to metal loss depth.

Peak amplitude in X direction (mV)	4057.74	3934.875	3897.711	3767.451	3705.173
Peak amplitude in Y direction (mV)	4043.544	3848.539	3692.336	3629.741	3532.597
Depth (mm)	0	−1	−2	−3	−4

the sensor is on the defect-free, the induced eddy current is uniform and the peak wave measured by the pickup coil is inherent. As shown in Figure 4(a), when the eddy currents in the specimen are disturbed by a defect whose resistance is bigger than that of the specimen material, they will flow to the two ends and the bottom of the defect. Consequently, the density of the eddy current on the defect ends is bigger than that of defect-free. The density of the eddy current on the bottom of the defect is smaller than that of defect-free because of skin effect. Therefore, as the probe scans along the defect, a crest will appear on the defect's end and a trough will appear on the defect's bottom. It is different when the sensor scans in the direction of the exciting current. As shown in Figure 4(b), the induced eddy current in the defect-free area is uniform. When eddy currents are disturbed by a defect whose resistance is bigger than that of the specimen, they will flow to the two sides and the bottom of the defect. Due to the skin effect, the eddy current density on the defect sides is bigger, while the density of the eddy current on the defect bottom is smaller than that of defect-free. Therefore, when the sensor scans on the two sides of the defect, a crest appears on the peak wave. In contrast, when the sensor scans along the center of the defect, a broad trough appears on the peak wave.

Defects 1 to 3 with simple shapes are used in the experiment. Peak waves of sensor scanning along the center of defects 1 to 3 in both directions are shown in Figures 5 and 6. The horizontal axis represents the location of the PEC sensor; the vertical axis represents the peak amplitude. The defect's location is from 80 mm to 120 mm. It can be seen from the plots that the peak waves are distorted as the defect is approached.

4.2. Depth versus Peak Amplitude. In both directions, peak waves present a broad trough along the center of the defect, which is likely to be relative to the defect's depth. Table 2 shows the peak amplitude corresponding to the defect depth in two directions. Experimental values in Table 2 are plotted in Figure 7, where the vertical axis represents the defect depth and the horizontal axis represents the peak amplitude. Apparently, with the increase of the absolute value of defect depth, peak amplitude reduces linearly, which provides an effective means to evaluate the depth of surface-breaking defects. The linear fitting lines are also shown in Figure 7. The goodness R^2 for fitted line in X direction is 0.9777, and the goodness R^2 for fitted line in Y direction is 0.9565. The linear formula to measure the defect depth in this experiment quantitatively is given by

$$d = 0.0112A_X - 45.392,$$
$$d = 0.0077A_Y - 30.906, \quad (1)$$

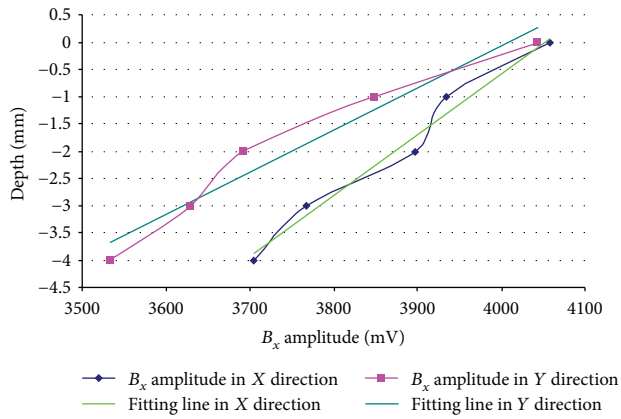

Figure 7: Measured value and fitting lines of peak amplitude and defect depth in different directions.

where d is the defect depth, A_X is the peak amplitude in X direction, and A_Y is the peak amplitude in X direction.

4.3. Depth Evaluation. In this section, the peak amplitudes are transformed to defect depth according to (1) to realize the defect evaluation. Defect depth profiles when the sensor scans along the center of defects 1 to 6 in X direction are shown in Figure 8, whilst defect depth profiles in Y direction are shown in Figure 9. The horizontal axis represents the location of the sensor; the vertical axis represents the estimated defect depth. It can be seen from Figures 8 and 9 that defect depth evaluation can be realized in both directions.

5. C-Scan-Based Metal Loss Imaging

Imaging technique can help us obtain the shape of defects and is more intuitive than traditional nondestructive testing methods. In recent years, some eddy current (EC) imaging methods are investigated to detect and evaluate the defects in metal structures, such as C-scan imaging, magneto-optical imaging [44], induction thermography [45–47], and electromagnetic induction tomography (EMT) [48]. In this section, the defects are evaluated based on the C-scan imaging.

The operation of C-scan imaging is controlled by the Windows-based domestic software, which is comprised of parameter setup, data acquisition, feature extraction, data process, and C-scan image display. Firstly, the parameters of excitation pulse are configured in the parameter setup. Then, the transient response signal measured using the B_x pickup coil is sampled in data acquisition. Next, in feature extraction, the peak amplitude of the transient

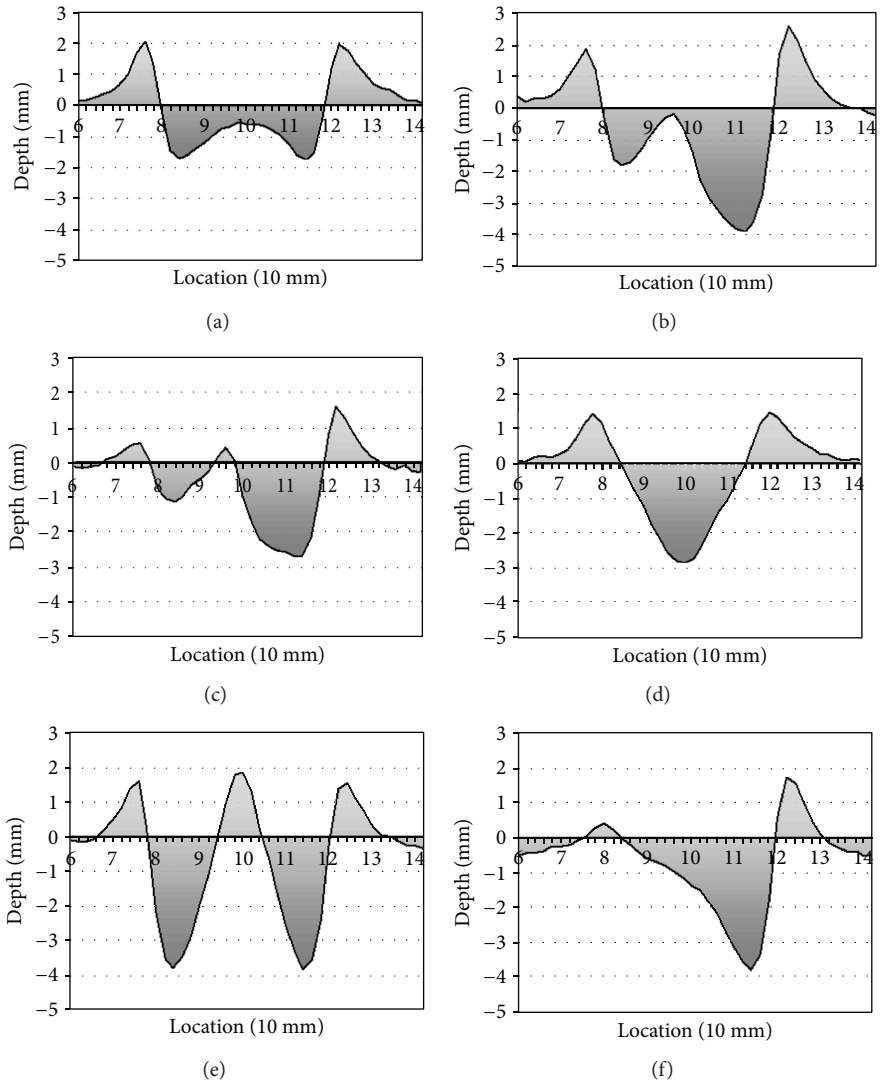

Figure 8: The depth evaluation of six defects in X direction. (a) Defect 1, (b) defect 2, (c) defect 3, (d) defect 4, (e) defect 5, and (f) defect 6.

response signal is extracted as the feature for C-scan imaging. In data process, the coordinate of the scanning point is determined and peak amplitude is transformed to depth and color according to the relationship between the peak amplitude and the defect depth. Consequently, the images of scanned areas are obtained during the step of C-scan image display and the sizing or the quantification of the defect is performed to gain information about the severity of the detected defect.

5.1. C-Scan Contour Images in Two Directions. The C-scan contour image of defect 4 in the direction of magnetic induction flux is shown in Figure 10, whilst the C-scan contour image of defect 4 in the direction of exciting current is shown in Figure 11. The horizontal axis represents the scanning path and the distance between the two adjacent scanning paths is 1 mm; the vertical axis represents the scanning time; the color bar represents the estimated defect depth. We can find that a trough will appear on the defect and a crest will appear on the defect end in the direction of magnetic induction flux in Figure 10 and that a trough will appear on the defect and a crest will appear on the defect sides in the direction of exciting current in Figure 11. The experimental results are consistent with the analysis in Section 4.1.

5.2. Metal Loss Evaluation Based on C-Scan Imaging. In this section, the C-scan imaging defect evaluation according to (1) is realized. Figure 12 shows the C-scan imaging results of four defects in the direction of magnetic induction flux, whilst Figure 13 shows the C-scan imaging results of four defects in the direction of the exciting current. The x-axis represents the scanning path; the y-axis represents the scanning time; the z-axis represents the estimated defect depth. The color bar represents the estimated depth, ranging from −5 mm to 3 mm. It can be seen from Figures 12 and 13 that the C-scan images of defects

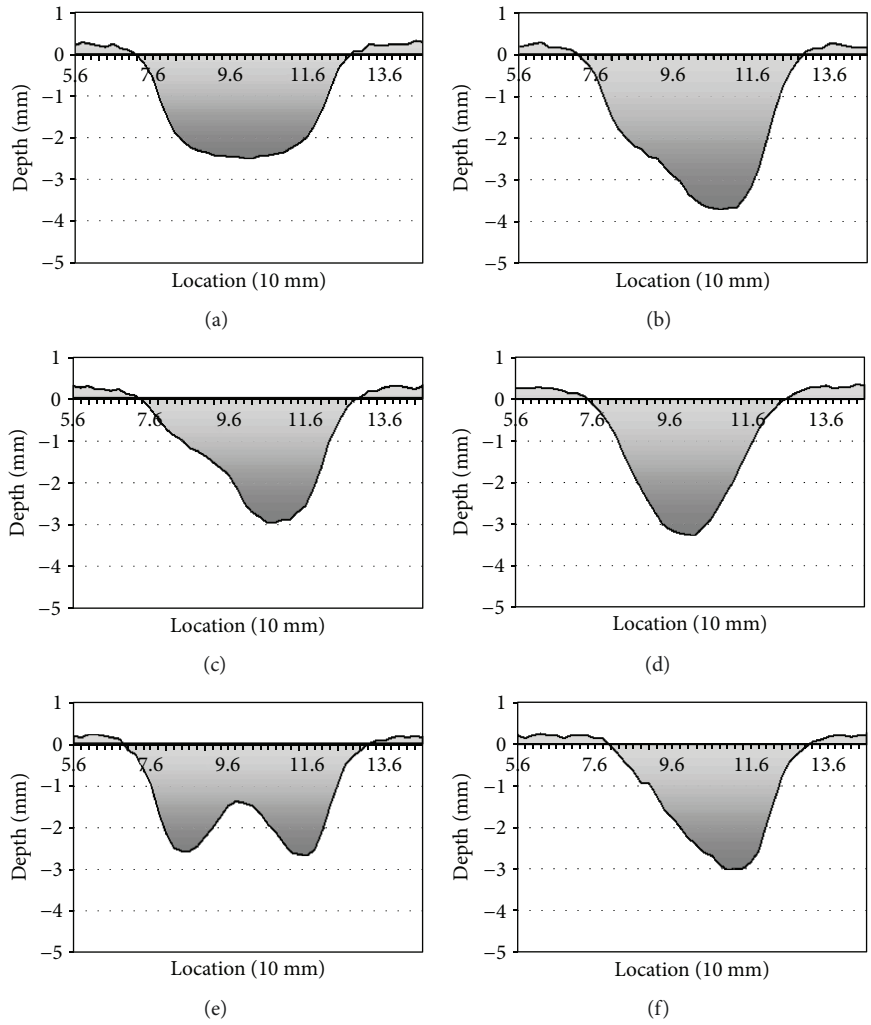

Figure 9: The depth evaluation of six defects in Y direction. (a) Defect 1, (b) defect 2, (c) defect 3, (d) defect 4, (e) defect 5, and (f) defect 6.

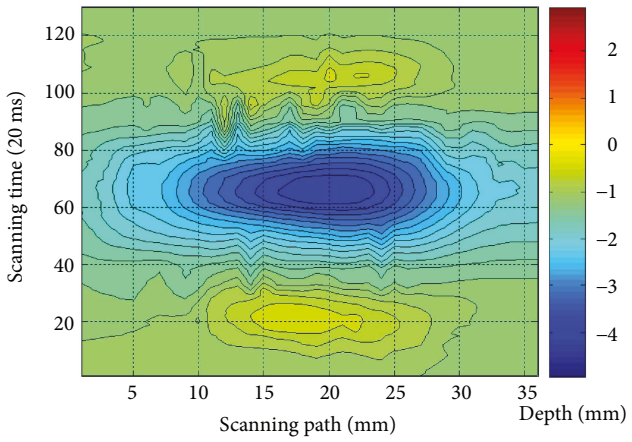

Figure 10: The C-scan contour images of defect 4 in direction of magnetic induction flux.

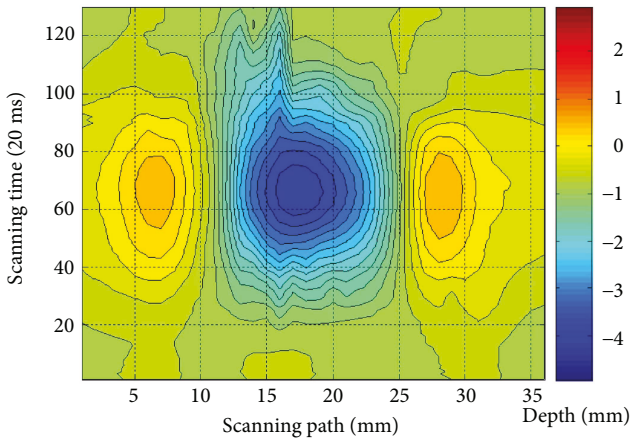

Figure 11: The C-scan contour images of defect 4 in direction of the exciting current.

present similar shape with the real defect. In other words, metal loss evaluation can be actualized in both directions of sensor scanning.

5.3. Sensitivity Comparison. The experimental results illuminate that the defects with different sections can be reconstructed in both directions. To evaluate the

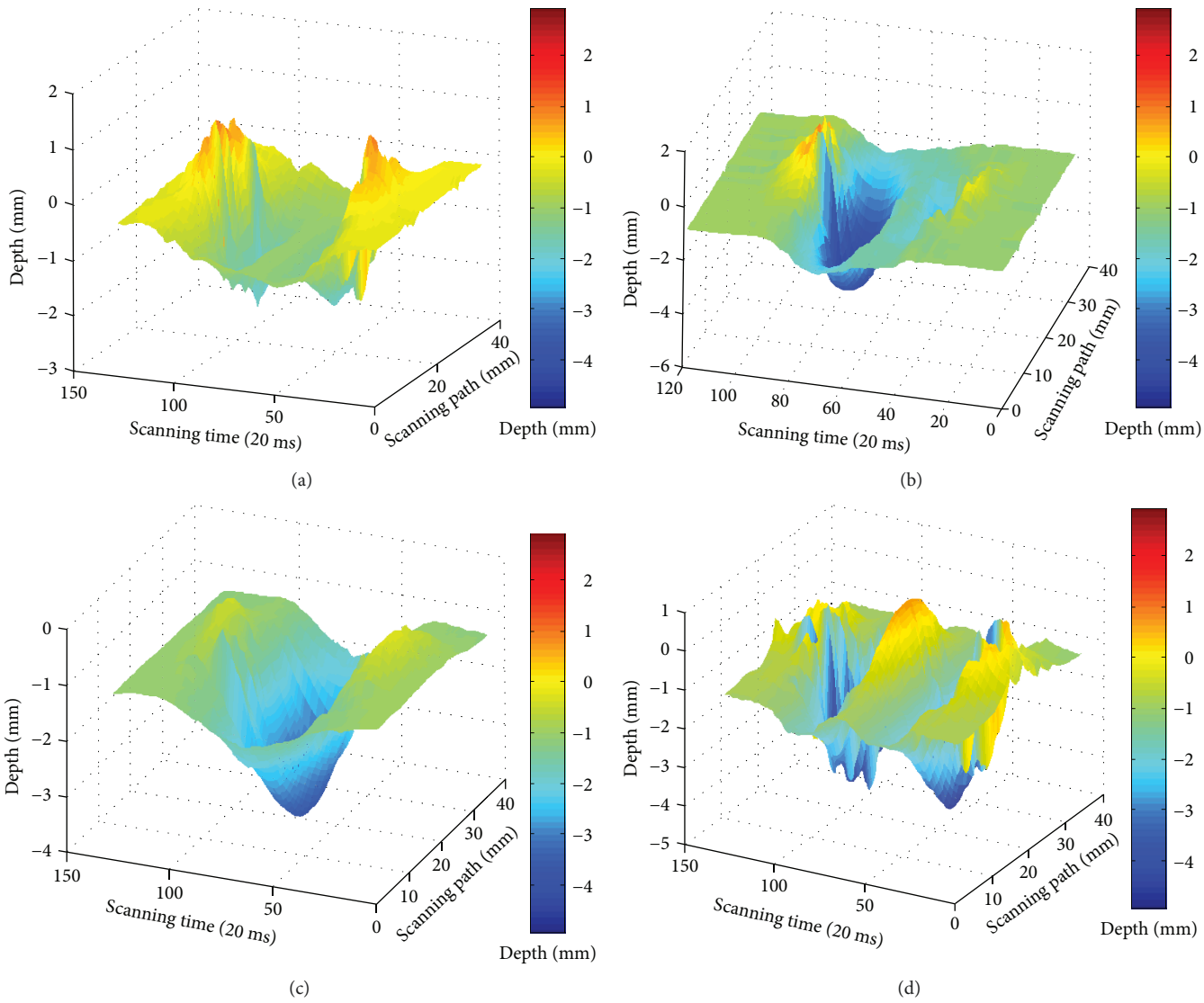

Figure 12: The C-scan 3D images of four defects in X direction. (a) Defect 1, (b) defect 2, (c) defect 4, and (d) defect 5.

performance of methods in the two directions, the C-scan results in the two directions are compared. Table 3 shows the minimum amplitude of defects in different scanning directions. Clearly, the changes in percentage by metal loss in the exciting current direction are a little bigger than those of the same metal loss in the magnetic induction flux direction. In other words, the metal loss type of defects can be detected in both directions.

6. Conclusions

In summary, this paper studied the PEC testing based on the rectangular excitation coil and the B_x pickup coil in the magnetic induction flux direction and the exciting current direction for the purpose of metal loss evaluation. Experimental results have illustrated that metal loss depth can be estimated effectively by the peak amplitude of the pickup coil. The metal loss depth quantification is preliminarily obtained based on the fitting equation, and metal loss evaluations are realized by peak waves and C-scan 3D images in both directions. In addition, the detection sensitivity in different directions is compared and the results illustrate that sensitivity in the exciting current direction is a little better than that in the magnetic induction flux direction. There is a fly in the ointment that the EDM slots simulating the metal loss by corrosion in this work are relatively big in dimension over the crack defect. Despite this, the proposed method based on the rectangular excitation coil and the axial parallel pickup coil is an effective approach to evaluate and image metal loss. In addition, the conductivity and lift-off between the sensor and the sample have not been considered in current work. We will further investigate the influence of conductivity and lift-off on our proposed probe and method. Defect detection and quantification of aluminum alloy materials, which are widely used in automobiles and aircrafts, is an

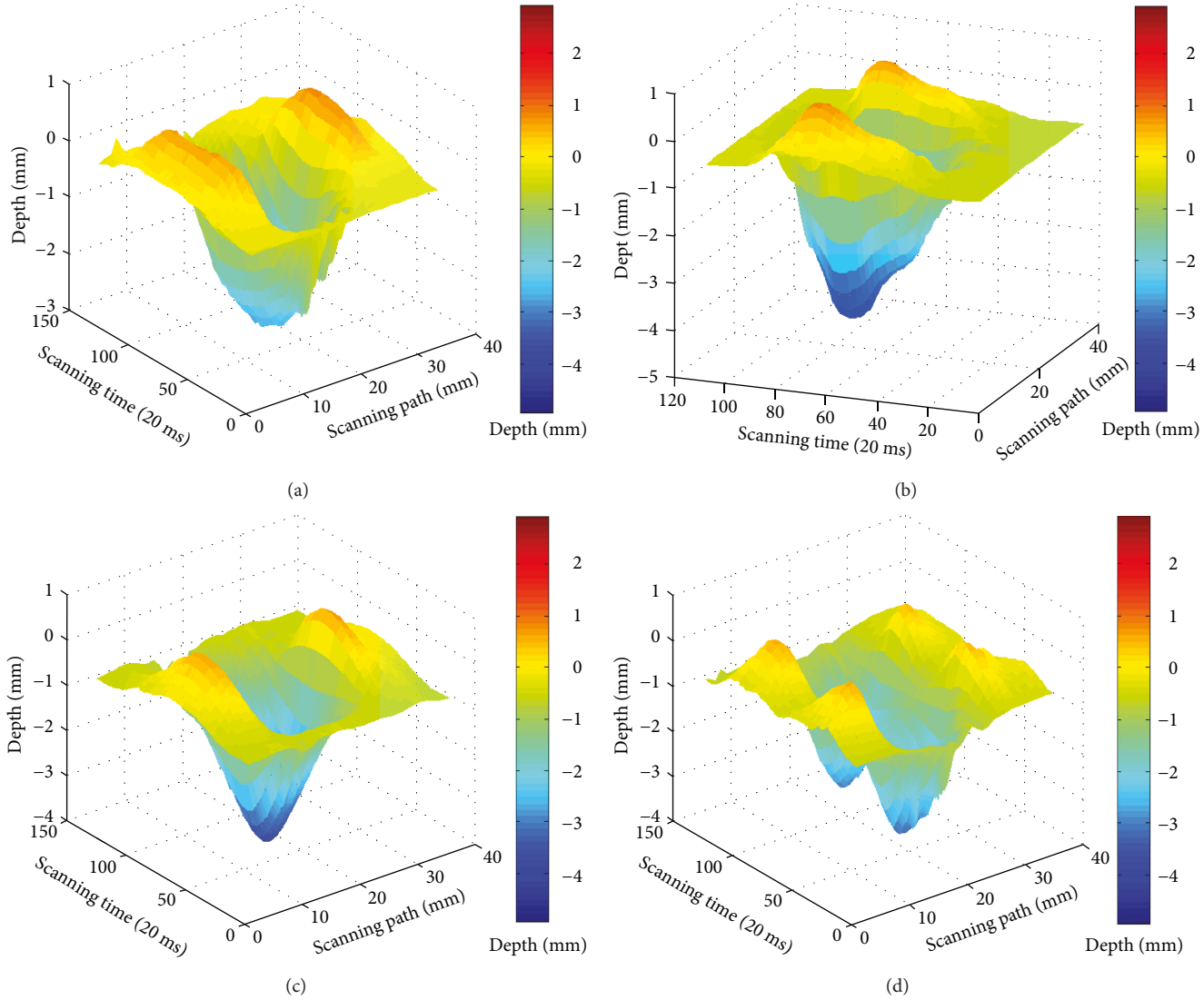

Figure 13: The C-scan 3D images of four defects in Y direction. (a) Defect 1, (b) defect 2, (c) defect 4, and (d) defect 5.

Table 3: Minimum peak amplitude of defects in two directions.

Scanning direction	Defect number	Defect 1	Defect 2	Defect 4	Defect 5
	No defect (mV)		4057.74		
X direction	Min. amplitude (mV)	3849.2	3636.1	3705.6	3663.1
	Pct. change	−5.14%	−10.39%	−8.68%	−9.73%
	No defect (mV)		4043.544		
Y direction	Min. amplitude (mV)	3645.9	3458.5	3499.3	3584.2
	Pct. change	−9.83%	−14.47%	−13.46%	−11.36%

important issue to be solved, and this method has the potential to be applied in the future.

Conflicts of Interest

The authors declare that they have no competing interests.

Acknowledgments

The work is supported by the Shenzhen Science and Technology Project (Basic research, Grant no. JCYJ 20170306144608417), National Natural Science Foundation of China (Grant no. 61501483), and the Shenzhen Basic Research Project (Grant no. JCYJ20160523113817077).

References

[1] F. Zi-jie, G. Liang-jin, and S. Rui-yi, "Research and development of automotive lightweight technology," *Journal of Automotive Safety and Energy*, vol. 5, no. 1, pp. 1–16, 2014.

[2] G. S. Cole and A. M. Sherman, "Light weight materials for automotive applications," *Materials Characterization*, vol. 35, no. 1, pp. 3–9, 1995.

[3] J. Hirsch and T. Al-Samman, "Superior light metals by texture engineering: optimized aluminum and magnesium alloys for automotive applications," *Acta Materialia*, vol. 61, no. 3, pp. 818–843, 2013.

[4] H. Jiang, P. Bowen, and J. F. Knott, "Fatigue performance of a cast aluminium alloy Al-7Si-Mg with surface defects," *Journal of Materials Science*, vol. 34, no. 4, pp. 719–725, 1999.

[5] J. Pan, "Casting defects analysis and improvement for bx15 cylinder head of automotive air conditioning compressor," *Foundry Technology*, vol. 32, no. 11, pp. 1494–1497, 2011.

[6] S. Y. Lee and B. H. Choi, "Effects of thixoforming defects on the stress-strain curves of aluminum structural parts for automobile," in *Solid State Phenomena*, pp. 743–748, Trans Tech Publ, 2008.

[7] T. D. Claar, C.-J. Yu, I. Hall, J. Banhart, J. Baumeister, and W. Seeliger, "Ultra-Lightweight Aluminum Foam Materials for Automotive Applications," *International Journal of Powder Metallurgy*, vol. 36, no. 6, pp. 61–+, 2000.

[8] R. J. Brown, "Non-destructive testing in industry," *Non-Destructive Testing*, vol. 6, no. 2, pp. 81–85, 1973.

[9] P. Buschke and W. Schappacher, "Trends in the automotive industry steer new NDT applications," *Insight-Non-Destructive Testing and Condition Monitoring*, vol. 48, no. 9, pp. 532–536, 2006.

[10] S. S. AHMED, A. KARAMALIS, and T. KOEPPEL, *Real-Time NDT of Automobile Bumpers with Millimeter-Wave Imaging Technology*, 19th World Conference on Non-Destructive Testing, 2016, http://www.ndt.net/search/docs.php3?showForm=off&id=19394.

[11] D. Zhou, J. Wang, Y. He, D. Chen, and K. Li, "Influence of metallic shields on pulsed eddy current sensor for ferromagnetic materials defect detection," *Sensors and Actuators A: Physical*, vol. 248, pp. 162–172, 2016.

[12] S. A. Titov, R. G. Maev, and A. N. Bogachenkov, "Pulse-echo NDT of adhesively bonded joints in automotive assemblies," *Ultrasonics*, vol. 48, no. 6-7, pp. 537–546, 2008.

[13] E. Schneider and C. Boller, "Non-destructive techniques and systems for process and quality Control in the automotive and supplier industry," in *Innovative Design, Analysis and Development Practices in Aerospace and Automotive Engineering*, pp. 11–11, Springer, 2014.

[14] Y. Li, X. Liu, Z. Chen, H. Zhao, and W. Cai, "A fast forward model of pulsed eddy current inspection of multilayered tubular structures," *International Journal of Applied Electromagnetics and Mechanics*, vol. 45, no. 1–4, pp. 417–423, 2014.

[15] A. Runnemalm and A. Appelgren, *Evaluation of Non-Destructive Testing Methods for Automatic Quality Checking of Spot Welds*, Automated quality checking of spot welds, 2012, http://www.diva-portal.org/smash/record.jsf?pid=diva2%3A642618&dswid=4353.

[16] J. Chen and Z. Feng, *IR-Based Spot Weld NDT in Automotive Applications*, Thermosense: Thermal Infrared Applications XXXVII, 2015, https://www.spiedigitallibrary.org/conference-proceedings-of-spie/9485/948513/IR-based-spot-weld-NDT-in-automotive-applications/10.1117/12.2177124.short?SSO=1.

[17] S. Bohm, M. Hellmanns, A. Backes, and K. Dilger, "Lock-in thermography based NDT of parts for the automotive industry," *Journal of Adhesion and Interface*, vol. 7, no. 4, pp. 10–12, 2006.

[18] A. Sophian, G. Y. Tian, D. Taylor, and J. Rudlin, "Design of a pulsed eddy current sensor for detection of defects in aircraft lap-joints," *Sensors and Actuators A: Physical*, vol. 101, no. 1-2, pp. 92–98, 2002.

[19] Y. He, G. Tian, H. Zhang, M. Alamin, A. Simm, and P. Jackson, "Steel corrosion characterization using pulsed eddy current systems," *IEEE Sensors Journal*, vol. 12, no. 6, pp. 2113–2120, 2012.

[20] M. Fan, P. Huang, B. Ye, D. Hou, G. Zhang, and Z. Zhou, "Analytical modeling for transient probe response in pulsed eddy current testing," *NDT & E International*, vol. 42, no. 5, pp. 376–383, 2009.

[21] M. Morozov, G. Y. Tian, and P. J. Withers, "Noncontact evaluation of the dependency of electrical conductivity on stress for various Al alloys as a function of plastic deformation and annealing," *Journal of Applied Physics*, vol. 108, no. 2, p. 024909, 2010.

[22] J. Wu, D. Zhou, and J. Wang, "Surface crack detection for carbon fiber reinforced plastic materials using pulsed eddy current based on rectangular differential probe," *Journal of Sensors*, vol. 2014, no. 5, Article ID 727269, 8 pages, 2014.

[23] R. A. Smith and G. R. Hugo, "Deep corrosion and crack detection in aging aircraft using transient eddy current NDE," in *Proc. 5th Joint NASA/FAA/DoD Aging Aircraft Conference*, 2001, https://www.researchgate.net/publication/228714020_Deep_corrosion_and_crack_detection_in_aging_aircraft_using_transient_eddy-current_NDE.

[24] R. Smith and G. Hugo, "Transient eddy current NDE for ageing aircraft-capabilities and limitations," *Insight: Non-Destructive Testing and Condition Monitoring*, vol. 43, no. 1, pp. 14–25, 2001.

[25] S. Giguère, B. A. Lepine, and J. M. S. Dubois, "Pulsed eddy current technology: characterizing material loss with gap and lift-off variations," *Research in Nondestructive Evaluation*, vol. 13, no. 3, pp. 119–129, 2001.

[26] B. A. Lepine, J. S. R. Giguere, D. S. Forsyth, A. Chahbaz, and J. M. S. Dubois, "Interpretation of pulsed eddy current signals for locating and quantifying metal loss in thin skin lap splices," *AIP Conference Proceedings*, vol. 615, no. 1, pp. 415–422, 2002.

[27] Y. He, M. Pan, and F. Luo, "Reduction of lift-off effects in pulsed eddy current for defect classification," *IEEE Transactions on Magnetics*, vol. 47, no. 12, pp. 4753–4760, 2011.

[28] X. Hu, Y. He, and F. Luo, "Defect classification in two-layer complex structures based on spectrum analysis of pulsed eddy current," *Insight - Non-Destructive Testing and Condition Monitoring*, vol. 53, no. 3, pp. 146–151, 2011.

[29] A. Sophian, G. Y. Tian, D. Taylor, and J. Rudlin, "A feature extraction technique based on principal component analysis for pulsed eddy current NDT," *NDT and E International*, vol. 36, no. 1, pp. 37–41, 2003.

[30] G. Yang, G. Y. Tian, P. W. Que, and T. L. Chen, "Independent component analysis-based feature extraction technique for defect classification applied for pulsed eddy current NDE,"

Research in Nondestructive Evaluation, vol. 20, no. 4, pp. 230–245, 2009.

[31] M. Pan, Y. He, G. Y. Tian, D. Chen, and F. Luo, "PEC frequency band selection for locating defects in two-layer aircraft structures with air gap variations," *IEEE Transactions on Instrumentation and Measurement*, vol. 62, no. 10, pp. 2849–2856, 2013.

[32] H. Hoshikawa and K. Koyama, "Non-destructive testing of weld zone with a uniform eddy current probe," *Insight*, vol. 40, no. 4, pp. 269–271, 1998.

[33] M. J. Knight, F. P. Brennan, and W. D. Dover, "Effect of residual stress on ACFM crack measurements in drill collar threaded connections," *NDT & E International*, vol. 37, no. 5, pp. 337–343, 2004.

[34] B. Yang, B. Li, and Y. Wang, "Reduction of lift-off effect for pulsed eddy current NDT based on sensor design and frequency spectrum analysis," *Nondestructive Testing and Evaluation*, vol. 25, no. 1, pp. 77–89, 2010.

[35] B. Lebrun, Y. Jayet, and J. C. Baboux, "Pulsed eddy current application to the detection of deep cracks," *Materials Evaluation*, vol. 53, no. 11, pp. 1296–1300, 1995.

[36] J. Kim, G. Yang, L. Udpa, and S. Udpa, "Classification of pulsed eddy current GMR data on aircraft structures," *NDT & E International*, vol. 43, no. 2, pp. 141–144, 2010.

[37] G. Y. Tian and A. Sophian, "Defect classification using a new feature for pulsed eddy current sensors," *NDT & E International*, vol. 38, no. 1, pp. 77–82, 2005.

[38] G. Panaitov, H. J. Krause, and Y. Zhang, "Pulsed eddy current transient technique with HTS SQUID magnetometer for non-destructive evaluation," *Physica C: Superconductivity*, vol. 372-376, no. 02, pp. 278–281, 2002.

[39] S. Li, S. Huang, and W. Zhao, "Development of differential probes in pulsed eddy current testing for noise suppression," *Sensors and Actuators A: Physical*, vol. 135, no. 2, pp. 675–679, 2007.

[40] H. C. Yang and C. C. Tai, "Pulsed eddy-current measurement of a conducting coating on a magnetic metal plate," *Measurement Science & Technology*, vol. 13, no. 8, pp. 1259–1265, 2002.

[41] Y. He, F. Luo, X. Hu, B. Liu, and J. Gao, "Defect identification and evaluation based on three-dimensional magnetic field measurement of pulsed eddy current," *Insight - Non-Destructive Testing and Condition Monitoring*, vol. 51, no. 6, pp. 310–314, 2009.

[42] Y. He, F. Luo, and M. Pan, "Defect characterisation based on pulsed eddy current imaging technique," *Sensors and Actuators A: Physical*, vol. 164, no. 1-2, pp. 1–7, 2010.

[43] Y. He, F. Luo, M. Pan, X. Hu, J. Gao, and B. Liu, "Defect classification based on rectangular pulsed eddy current sensor in different directions," *Sensors and Actuators A: Physical*, vol. 157, no. 1, pp. 26–31, 2010.

[44] P. Y. Joubert and J. Pinassaud, "Linear magneto-optic imager for non-destructive evaluation," *Sensors and Actuators A: Physical*, vol. 129, no. 1-2, pp. 126–130, 2006.

[45] B. Gao, W. L. Woo, and Y. T. Gui, "Electromagnetic thermography nondestructive evaluation: physics-based modeling and pattern mining," *Scientific Reports*, vol. 6, no. 1, article 25480, 2016.

[46] Y. He, R. Yang, H. Zhang, D. Zhou, and G. Wang, "Volume or inside heating thermography using electromagnetic excitation for advanced composite materials," *International Journal of Thermal Sciences*, vol. 111, pp. 41–49, 2017.

[47] R. Yang and Y. He, "Optically and non-optically excited thermography for composites: a review," *Infrared Physics & Technology*, vol. 75, pp. 26–50, 2016.

[48] X. Ma, A. J. Peyton, S. R. Higson, A. Lyons, and S. J. Dickinson, "Hardware and software design for an electromagnetic induction tomography (EMT) system for high contrast metal process applications," *Measurement Science & Technology*, vol. 17, no. 1, pp. 111–118, 2006.